Tuijin Jishu/Journal of Propulsion Technology
ISSN: 1001-4055
Vol. 44 No. 6 (2023)

Synthesis, structural, morphology, and vibrational properties of Ba^{2+} doped $BiFeO_3$ multiferroic materials

[1*] G. M. Sravani, [2] B. Chandra Sekhar, [3] P. S. V. Shanmukhi, [4] Praveen Choppara, [5] P. Himakar, [6] K. Samatha

[1] [6] Department of Physics, Andhra University, Visakhapatnam, A. P., India
[2] Vignan's Institute of Engineering for Women, Visakhapatnam, A. P., India
[3] Department of Physics, Aditya College of Engineering and Technology, Surampalem, India.
[4] Department of Chemistry, P. R. Degree College (A), Kakinada-533001, A. P., India.
[5] Department of Physics, P. R. Degree College (A), Kakinada-533001, A. P., India.

*Corresponding author: gokadamanikantasravani@gmail.com

Abstract: This paper investigates the structural, morphological, and vibrational characteristics of sol-gel auto-combustion $Bi_{1-x}Ba_xFe_2O_3$ (x = 0.00, 0.05, 0.1, 0.15, 0.2, and 0.25) multiferroics. Characterization of the synthesized samples was accomplished using X-ray diffraction (XRD), field emission scanning electron microscopy (FESEM) and Fourier-transform infrared spectroscopy (FTIR). They have a rhombohedral structure with the R3c space group. FESEM experiments showed the nanocrystalline nature of prepared materials. The Fe-O bond vibrations of about 450–465 and 560–582 cm^{-1} are seen in the FTIR spectra.
Keywords: Nanomaterials; Doped BFO; Crystal structure.

1. Introduction

The prospective applications of multiferroic materials in information storage have garnered significant attention [1-3]. These materials include ferroelectric and ferromagnetic (or antiferromagnetic) ordering in a single phase and magnetoelectric interaction between them [4]. These materials are uncommon in ABO_3-type perovskite materials; nevertheless, they require empty or partially filled transition metal d-orbitals to simultaneously have both ferromagnetic and ferroelectric—mutually exclusive properties [5]. From a practical application perspective, $BiFeO_3$ (BFO) is the most promising of these rare ABO_3-types of perovskite multiferroic materials because of its relatively high ferroelectric Curie (TC 1103 K for bulk BFO) and G-type antiferromagnetic Neel (TN 643 K for bulk BFO) temperatures, which exhibit multiferroic behaviors at room temperature [6]. Numerous recent investigations have been published on the ferromagneticity and ferroelectricity characteristics of BFO ceramic and nanostructure materials. Unfortunately, potential applications of BFO are hampered by some significant issues related to electrical and multiferroic characteristics [7]. As such, there are still issues that need to be resolved, such as (1) inhomogeneous weak magnetization, (2) high leakage current density, (3) poor ferroelectric dependability, and (4) weak ferroelectric remanent polarization. As a result, several efforts have been made to get around these challenges [8]. BFO nanoparticles display notable property variations compared to their bulk counterparts because of the size effect and huge surface-to-volume ratio [9].

Because $BiFeO_3$ has both ferroelectric and antiferromagnetic characteristics and record-high Curie and Neel temperatures (TC = 1103 K, TN = 643 K), it is one of the most significant single-phase multiferroic materials [10]. Because of these remarkable qualities, $BiFeO_3$ can be used in various industries, including digital recording, radio, television, microwave satellite communication, bubble memory devices, audio-video, sensors, optical filters, smart devices, and high-density ferroelectric random access memory [11-14]. The ABO_3 type rhombohedral distorted perovskite structure with R3c space group describes its crystal structure. The distorted rhombohedral structure of $BiFeO_3$ is a spin cycloid with an in commensurate long wavelength period of 62 nm, which prevents the linear magnetoelectric effect and cancels out the macroscopic magnetism [15]. To address this issue, several strategies have been tested, including the substitution of A and B sites in the $BiFeO_3$

perovskite structure (ABO_3) to either enhance optical properties, ferroelectricity, and/or ferromagnetism or prevent secondary phases and Bi volatilization. Another strategy is to prepare $BiFeO_3$ solid solutions with other appropriate compounds, which prevents the formation of a secondary phase and improves its features [17].

It has been observed that the physical properties of other ABO_3 types of perovskite materials, such as the piezoelectric properties of Ba-modified $KNbO_3$ ceramics, can be effectively improved by substituting the alkali element Ba [18]. The samples' electrical, magnetic, and structural characteristics were thoroughly examined. Owing to charge neutrality, the number of holes or electron carriers and oxygen vacancies in BFO can be easily influenced by substituting aliovalent elements, such as Ca^{2+}, Ba^{2+}, Sr^{2+}, Ni^{2+}, etc., at the trivalent Bi-site or Fe-site [19-21]. Chemical approaches are among the most versatile as they offer control over the conditions and parameters of crystal development, deformation, thermal expansion, and chemical doping. Several noteworthy chemical processes include mechanosynthesis, Sol-gel, Pechini's method, hydrothermal, sonochemistry, and combustion synthesis [22-24]. Nevertheless, characteristics like electrical and magnetic qualities do not behave as predicted because these processes frequently involve obtaining nanoscale materials, implying the need to improve various aspects of these synthetic routes given the vast number of variables that must be controlled [25]. Several studies have investigated the doping of BFO with Ba^{2+} to achieve stable phases by the sol-gel method. However, reports utilizing alternative synthesis methods are uncommon. Because of this, the current study offers an organized, affordable, and practical way to produce materials based on a $BiFeO_3$ host structure that Ba^{2+} ions have altered [26].

This work reports the practical synthesis of $Bi_{1-x}Ba_xFeO_3$ MNPs for x = 0.0, 0.05, 0.1, 0.15, 0.2 and 0.25 samples prepared by sol-gel auto combustion technique. A thorough analysis of the impact of Ba^{2+} content on the phase structure, vibrational mode, size, and morphology was conducted.

2. Experimental studies

Sol-gel auto-combustion synthesis was used to examine the nanocrystallines of $Bi_{1-x}Ba_xFeO_3$ (BBFO), where x = 0.0, 0.05, 0.10, 0.15, 0.20, and 0.25, respectively. The analytical-grade starting materials, $Bi(NO_3)_3{\cdot}5H_2O$, $Fe(NO_3)_3{\cdot}9H_2O$, and $Ba(NO_3)_2$, were utilized without additional purification. Citric acid dissolved in the appropriate stoichiometric ratios in 1:1 M. The heated powders were annealed for 30 minutes at 650 °C. Pellets were polished and coated with silver paste on their surfaces to serve as electrodes for measuring the dielectric constant and loss tangent.

Using X-ray diffraction (XRD) (D8 Advanced, Bruker, Karlsruhe, Germany), the crystal structure and microstructural characteristics of BBFOx nanocrystallines were assessed at room temperature. Grain size distribution and microstructure morphology were assessed using field emission scanning electron microscopy (FESEM, JEOL JSM-7401F) and a 30 kV field emission gun.

3. Results and discussion

3.1 XRD analysis

From X-ray diffraction (XRD), Ba-doped BFO where x = 0.0, 0.05, 0.10, 0.15, 0.20, and 0.25 sample patterns were obtained and shown in Figure 1. All of the diffraction peaks in the patterns correspond to a rhombohedral structure that is part of the R3c space group, which is reported for BFO and is indexed using a hexagonal cell [27]. The study of the distorted rhombohedral structure as a function of Ba content (as per the JCPDS card 74–1098) can be conducted using the doublet nature of planes (104) and (110) in the $31° < 2\theta < 33°$ range [28]. This distortion is attributed to charge compensation, which nearly vanishes at higher dopant concentrations. The cation of dopants Since Ba^{2+} has a little larger ionic radius Ba^{2+} (1.18 Å) than Bi^{3+} (1.17 Å), it is reasonable to assume that when the concentration of Ba^{2+} in $BiFeO_3$ nanoparticles increases, the lattice constant values will decrease [29].

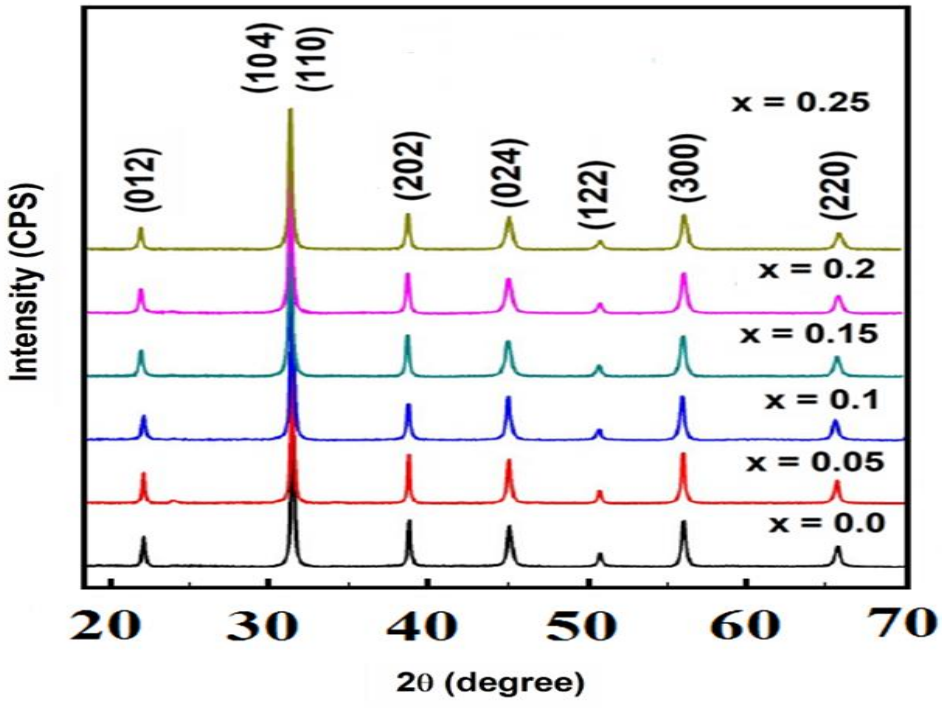

Figure 1: XRD patterns of $Bi_{1-x}Ba_xFeO_3$ multiferroics

Table 1: Structural parameters of $Bi_{1-x}Ba_xFeO_3$ multiferroics

Compounds	x = 0.0	x = 0.05	x = 0.1	x = 0.15	x = 0.2	x = 0.25
a (Å)	5.535	5.541	5.563	5.634	5.662	5.681
c (Å)	13.67	13.61	13.56	13.50	13.46	13.43
c/a (Å)	2.47	2.51	2.47	2.43	2.40	2.36
Crystallite size (nm)	28.62	26.82	24.98	21.95	18.85	16.35

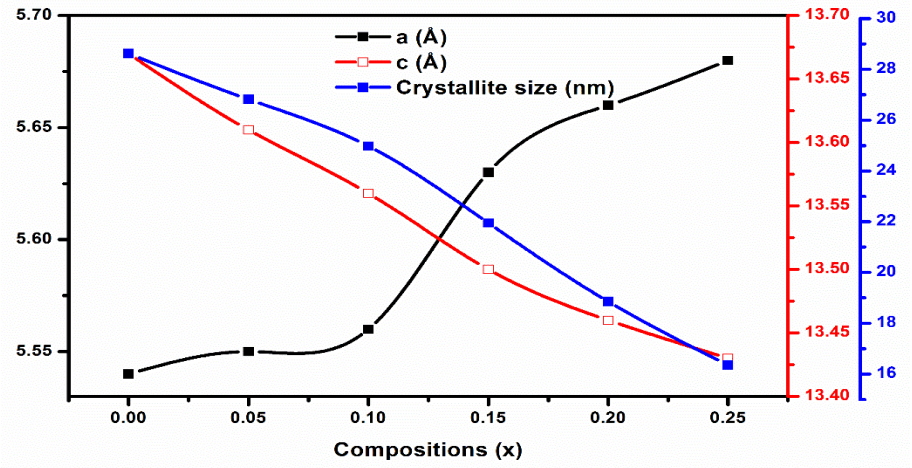

Figure 2: Lattice constant vs. crystallite size values of $Bi_{1-x}Ba_xFeO_3$ multiferroics

Strain relaxation in the materials containing dopant additions can be linked to the little shift in the primary peak location to lower angles observed with a slight increase in dopant concentration compared to pure BFO. The statistics from Ref. [30] and the current results agree. Because of the internal tension that the Ba ions

create in the perovskite structure of BFO, the more excellent value of the Ba^{2+} ionic radius compared to the Bi^{3+} ionic radius can help to explain this slight displacement.

Table 1 and Figure 2 show and list every lattice parameter and crystallite size value. The tabulated parameters make it clear that an increase in doping results in an increase in lattice parameter a, but there is no systematic fluctuation in lattice parameter c. However, an increase in doping has been associated with an improvement in unit cell volume. This could be because Ba^{2+} has a bigger ionic radius than Bi^{3+}. Additionally, the XRD pattern shows that the average full width at half maxima, or FWHM, value increases with increasing doping levels before decreasing at higher doping levels. A high FWHM value indicates a very small crystallite size, which could break the spiral spin structure and lessen the $BiFeO_3$ system's leaky characteristic [31].

Scherrer's formula determined the average crystallite size of the produced nanocrystalline $Bi_{1-x}Ba_xFeO_3$ samples [32]

$$\mathbf{D} = \frac{K\lambda}{\beta_{hkl}Cos(\theta_{hkl})}$$

Where K is the shape factor valued at 0.9, λ is the wavelength of Cu kα XRD, and β_{hkl} the Full Width at Half Maxima (FWHM). Crystallite size in BBFO materials decreases with Ba^{2+} substitutions compared to pure BFO.

3.2 FESEM analysis

$Bi_{1-x}Ba_xFeO_3$ (x = 0.00, 0.05, 0.10, 0.15, 0.2 and 0.25) nanostructured samples' FESEM micrographs are shown in Fig. 3. These micrographs demonstrate the relatively dense morphology of almost spherical grains, with sizes ranging from 30 to 95 nm, seen in nanostructured materials. The results of the XRD investigation [33] and the decreasing grain size with increasing dopant concentration in $BiFeO_3$ are similar. Particle development is inhibited, and the lattice enhances the nucleation rate in the system stresses [34]. In $Bi_{1-x}Ba_xFeO_3$ ceramics, the doping concentration increases with a corresponding decrease in grain size. The reduction in oxygen vacancy concentration can explain the decrease in grain size of $Bi_{1-x}Ba_xFeO_3$ ceramics.

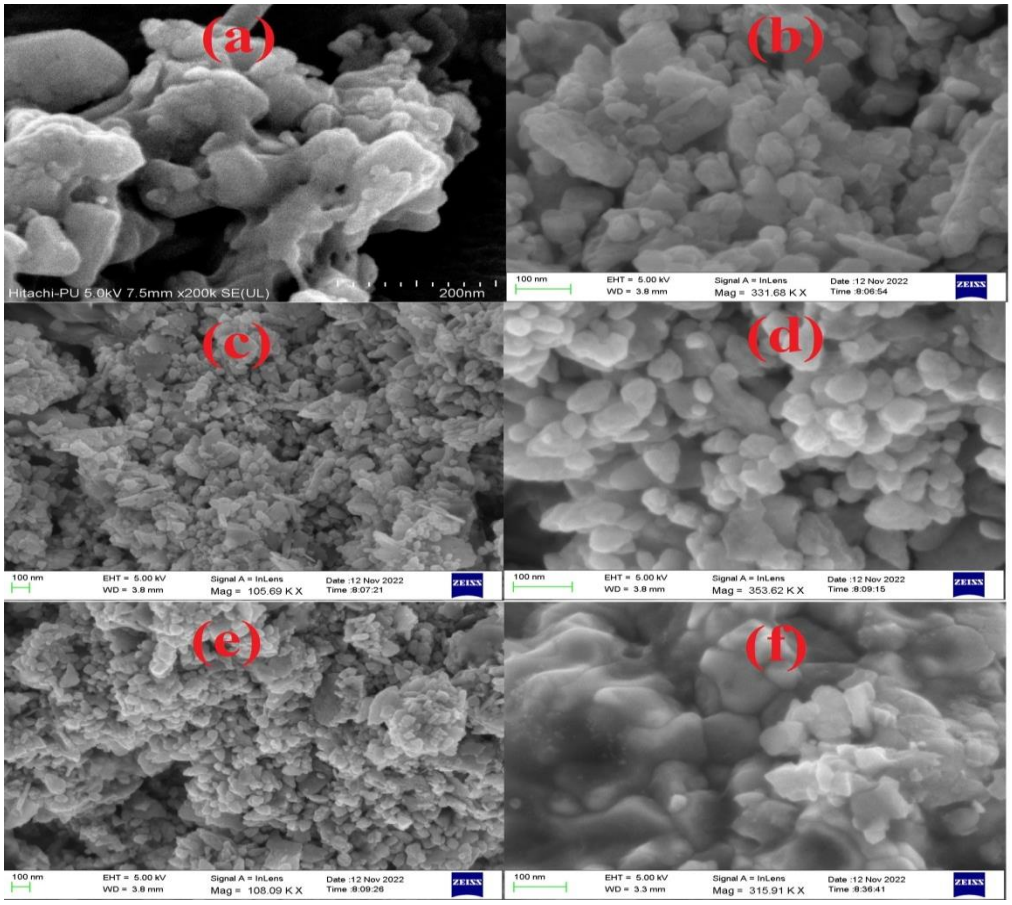

Figure 3: FESEM images of $Bi_{1-x}Ba_xFeO_3$ multiferroics

3.3 FTIR analysis

The vibrational characteristics of Ba-doped $BiFeO_3$ (x = 0.00, 0.05, 0.10, 0.15, 0.2 and 0.25) nanoparticles were examined through Fourier-transform infrared (FTIR) spectroscopy. In the perovskite structure, notable absorption peaks at approximately 450-465 and 560-582 cm^{-1} indicate the stretching vibrations of the Fe-O bond in the tetrahedral site for FeO_4 and the octahedral site for FeO_6, as depicted in Figure 4. Ba-doped BFO exhibits octahedral FeO_6 modes at around 560-582 cm^{-1}. The tetrahedral shows compressing Fe-O vibration at around 450–465 cm^{-1}, whereas the octahedral groups move from 582 cm^{-1} to 560 cm^{-1}. In any case, we attribute the absorption band traces seen at about 600 cm^{-1} to the Fe-O stretching vibrations of the FeO_6 group in the perovskite compounds [35]. The augmentation in calcination temperature is evident in the broadening and intensification of peaks at approximately 810 cm^{-1} in BFO materials [36] and peaks ranging from 815-822 cm^{-1} in our samples of Ba-doped BFO. This phenomenon indicates an escalation in crystallite volume.

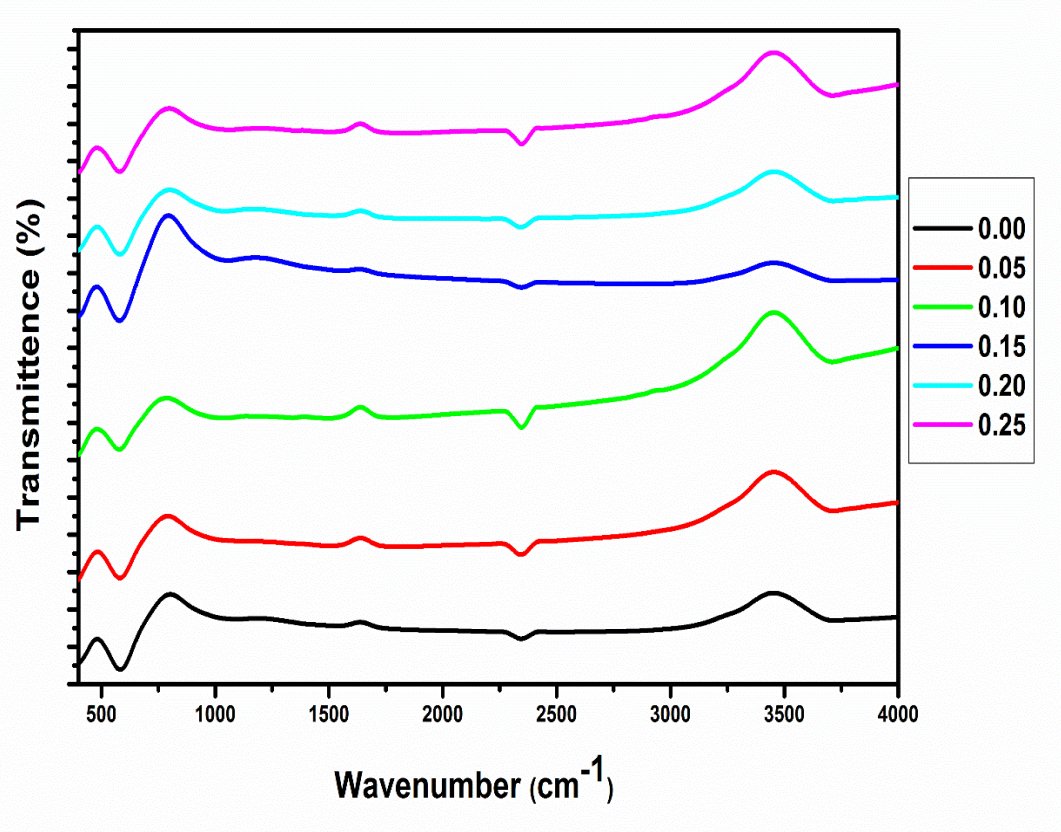

Figure 4: FTIR micrograph of $Bi_{1-x}Ba_xFeO_3$ multiferroics

Similarly, the band within the range of 800-1000 cm^{-1} signifies the crystalline phase of the metal-oxygen bond, while the band around 1000 cm^{-1} corresponds to the vibrations of the Bi-O and Ba-O bonds. The H_2O and OH stretching bond antisymmetric and symmetric peak positions are found between 3000 cm^{-1} and 3600 cm^{-1}, and the vibrating H_2O group is found between 1500 cm and 1650 cm^{-1} [37]. At 1400 cm^{-1}, the trapped nitrates are indicated. The presence of nitrate ions is most likely indicated by the band centred at approximately 2362 cm^{-1} [38]. The peaks detected at around 2852 and 2900 cm^{-1} are attributed to stretching vibrations of C-H symmetric [39]. For all samples, the measured spectrum shows the presence of metal-oxide bands, indicating that the BBFO have crystallized in a perovskite structure. There was no discernible peak shifting as a result of the barium doping. Several higher wavenumber impurity absorption peaks occur because of surface-adsorbed organic precursors during the synthesis or characterisation procedures. The high surface-to-volume ratio of nanoparticles makes these organic contaminants more dominating, while the peaks of these impurities gradually disappear in bulk samples [40].

4. Conclusions

The well-known sol-gel auto-combustion synthesis method was used to prepare $Bi_{1-x}Ba_xFeO_3$ (x = 0.00, 0.05, 0.1, 0.15, 0.2, and 0.25) multiferroic nanoparticles, after which their structural and magnetic characteristics were examined. Results from the structural and magnetic characteristics demonstrated that altering the doping values caused the size of the nanoparticles to shrink and the ferromagnetic properties to rise. Ba doping enhances crystallinity, and the XRD patterns demonstrate that practically all samples are crystalline. Doping led the XRD peaks to shift to the higher angle side, indicating that the structure of the BFO has been slightly altered. FESEM morphology of nanoparticles indicates that the grains are virtually spherical, which reduces grain size.

References

[1] G. Catalan, J.F. Scott, Adv. Mater. 21 (2009) 2463.
[2] H. Béa, M. Gajek, M. Bibes, A. Barthélémy, J. Phys. Condens. Matter 20 (2008) 434221.
[3] J.F. Scott, Nat. Mater. 6 (2007) 256.
[4] W. Eerenstein, N.D. Mathur, J.F. Scott, Nature 442 (2006) 759.
[5] Y.P. Wang, L. Zhou, M.F. Zhang, X.Y. Chen, J.-M. Liu, Z.G. Liu, Appl. Phys. Lett. 84 (2004) 1731.
[6] J.L. Mukherjee, F.F.Y. Wang, J. Am. Ceram. Soc. 54 (1971) 31.
[7] T. Park, G.C. Papaefthymiou, A.J. Viescas, A.R. Moodenbaugh, S.S. Wong, Nano Lett. 7 (2007) 766.
[8] S. Li, Y. Lin, B. Zhang, Y. Wang, C. Nan, J. Phys. Chem. C 114 (2010) 2903.
[9] S.K. Srivastav, N. S. Gajbhiye, J. Am. Ceram. Soc. 95 (2012) 3678.
[10] S.H. Han, K.S. Kim, H.G. Kim, H. Lee, H. Kang, J.S. Kim, C. Il Cheon, Ceram. Int. 36 (2010) 1365.
[11] N. Das, R. Majumdar, A. Sen, H.S. Maiti, Mater. Lett. 61 (2007) 2100.
[12] I. Szafraniak, M. Połomska, B. Hilczer, A. Pietraszko, L. Kępiński, J. Eur.Ceram. Soc. 27 (2007) 4399.
[13] G. Rojas-George, J. Silva, R. Castañeda, D. Lardizábal, O.A. Graeve, L. Fuentes, A. Reyes-Rojas, Mater. Chem. Phys. 146 (2014) 73.
[14] E.C. Aguiar, M.A. Ramirez, F. Moura, J.A. Varela, E. Longo, A.Z. Simões, Ceram. Int. 39 (2013) 13.
[15] J. Xu, H. Ke, D. Jia, W. Wang, Y. Zhou, J. Alloys Compd. 472 (2009) 473.
[16] J. Yang, X. Li, J. Zhou, Y. Tang, Y. Zhang, Y. Li, J. Alloys Compd. 509 (2011) 9271.
[17] C. Oommen, S.R. Jain, J. Hazard. Mater. A67 (1999) 253.
[18] Subba Rao GV, Rao CNR, Appl. Spectrosc. 24 (1970) 436.
[19] C. Chen, J. Cheng, S. Yu, L. Che, Z. Meng, J. Cryst. Growth 291 (2006) 135.
[20] P. Pandit, S. Satapathy, P.K. Gupta, V.G. Sathe, J. Appl. Phys. 106 (2009) 114105.
[21] J. Park, M.D. Le, J. Jeong, S. Lee, J. Phys. Condens. Matter 26 (2014) 433202.
[22] F. Gao, X.Y. Chen, K.B. Yin, S. Dong, Z.F. Ren, F. Yuan, T. Yu, Z.G. Zou, J.-M. Liu, Adv. Mater. 19 (2007) 2889.
[23] C. Elissalde, J. Ravez, J. Mater. Chem. 11 (2001) 1957.
[24] G. Ray, N. Sinha, B. Kumar, Mater. Chem. Phys. 142 (2013) 619.
[25] M.K. Gupta, B. Kumar, J. Alloys Compd. 509 (2011) L208.
[26] M.G. Masud, A. Ghosh, J. Sannigrahi, B.K. Chaudhuri, J. Phys. Condens.Matter 24 (2012) 295902.
[27] A. Singh, V. Pandey, R. Kotnala, D. Pandey, Phys. Rev. Lett. 101 (2008) 247602.
[28] H. Singh, K.L. Yadav, J. Phys. Condens. Matter 23 (2011) 385901.
[29] V.R. Palkar, J. John, R. Pinto, Appl. Phys. Lett. 80 (2002) 1628.
[30] Z. Huang, Y. Cao, Y. Sun, Y. Xue, C. Chu, Phys. Rev. B 56 (1997) 2623.
[31] T. Durga Rao, R. Ranjith, S. Asthana, J. Appl. Phys. 115 (2014) 124110.
[32] S. Kumari, N. Ortega, A. Kumar, S.P. Pavunny, J.W. Hubbard, C. Rinaldi, G. Srinivasan, J.F. Scott, R.S. Katiyar, J. Appl. Phys. 117 (2015) 114102.
[33] K. Funke, Prog. Solid St. Chem. 22 (1993) 111.
[34] S.K. Pradhan, B.K. Roul, Phys. B Condens. Matter 407 (2012) 2527.
[35] G.W. Pabst, L.W. Martin, Y.-H. Chu, R. Ramesh, Appl. Phys. Lett. 90 (2007) 072902.
[36] A.K. Pradhan, K. Zhang, D. Hunter, J.B. Dadson, G.B. Loiutts, P. Bhattacharya, R. Katiyar, J. Zhang, D.J. Sellmyer, U.N. Roy, Y. Cui, a. Burger, J. Appl. Phys. 97 (2005) 093903.

[37] M.M. Kumar, V.R. Palkar, K. Srinivas, S. V. Suryanarayana, Appl. Phys. Lett. 76 (2000) 2764.
[38] J. Wang, J.B. Neaton, H. Zheng, V. Nagarajan, S.B. Ogale, B. Liu, D. Viehland, V. Vaithyanathan, D.G. Schlom, U. V. Waghmare, N.A. Spaldin, K.M. Rabe, M. Wuttig, R. Ramesh, Science 299 (2003) 1719.
[39] J. Wu, J. Wang, D. Xiao, J. Zhu, ACS Appl. Mater. Interfaces 4 (2012) 1182.
[40] B.-C. Luo, C.-L. Chen, Z. Xu, Q. Xie, Phys. Lett. A 374 (2010) 4265.